UNITED NATIONS UNIVERSITY
UNU-GTP
Geothermal Training Programme

Orkustofnun, Grensasvegur 9,
IS-108 Reykjavik, Iceland

Reports 2016
Number 16

MONITORING MICRO-EARTHQUAKES IN A GEOTHERMAL FIELD

Fahman Hassan Abdallah
Djiboutian Development Office of Geothermal Energy – ODDEG
P.O. Box 1279
Djibouti
REPUBLIC OF DJIBOUTI
fahman.abdallah@gmail.com

ABSTRACT

Passive seismic technique is one of several geophysical methods used to understand structures in subsurface geology. This technique can be used in geothermal exploration to delineate faults in areas of geothermal activity, and to locate permeable zones within the geothermal system. During the exploitation of a geothermal system, measurements of microseismicity are useful to monitor the response of the system to fluid injection and production. Injection can increase the level of microseismicity in an area by increasing the pore pressure, and thereby reducing the effective stress.

In this study, the discussion is mainly based on monitoring of microearthquakes in the Hellisheidi geothermal system, located in the Hengill volcanic system. The area is located at the triple junction of two spreading zones and a transform zone and is therefore both tectonically and seismically active. The data set used in this report is a part of a larger dataset recorded by a local seismic network operated in the Hengill area by the Iceland GeoSurvey (ÍSOR), Uppsala University, MIT, Reykjavik University, and the Iceland Meteorological Office (IMO) from 2009-2013. In this report, data from a small swarm on April 25th, 2012, were analysed using SeisComP3.

A brief overview of microseismic surveys undertaken in the Hanle-Gaggade area in Djibouti is presented, describing the relationship between microearthquakes and signs of geothermal activity in the area. Earthquakes concentrated near the fault systems are observed, confirming that the area is seismically active and a local seismic network would be recommended for monitoring.

1. INTRODUCTION

Geophysical methods are one of the geoscientific disciplines that allow us to understand subsurface structures. For geothermal exploration, they are divided into direct methods and indirect methods. Direct methods include thermal and electrical methods that measure physical properties like temperature and resistivity directly in subsurface layers. The layers can be affected by alteration or salinity caused by underground natural resources like oil, water or geothermal fluid. Indirect methods or structural methods

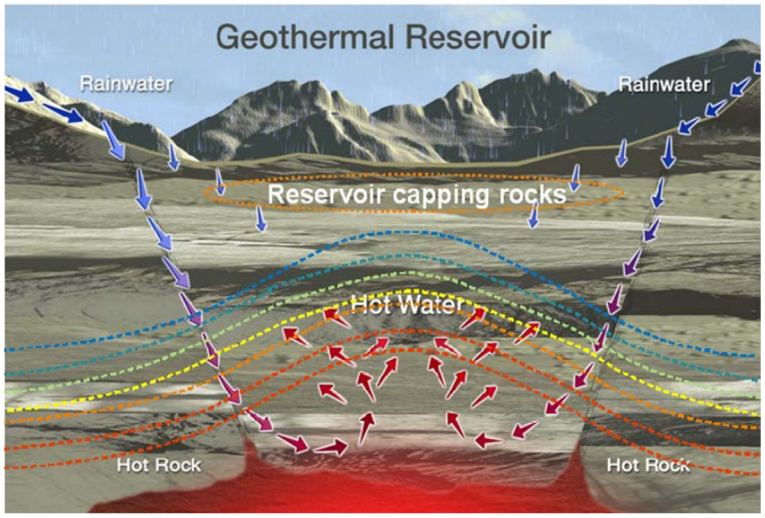

FIGURE 1: Components of a geothermal system: differently shaded/coloured dotted lines show different temperatures as the water heats up with depth (Geothermal Education Office, 2007)

include seismic, gravity and magnetic methods which detect anomalies associated with geological formations or structures (e.g. fault, dykes, or intrusions). In geothermal exploration these methods play an important role in locating and or assessing a geothermal system.

Geothermal systems are characterized by three basic components: a heat source, a reservoir, and conduits or pathways to allow circulation of fluid (Wanjohi, 2007). Where impermeable cap rock is present the geothermal system can be pressurized (Figure 1).

Geothermal areas are often associated with microearthquake activity (Foulger and Julien, 2009), making seismic methods a valuable exploration tool for the general understanding and monitoring of geothermal fields. In this report, the discussion is mainly based on monitoring microearthquakes in geothermal fields using passive seismic techniques. This technique is based on vibrations from natural earthquakes and its aim is to determine the hypocentre of earthquakes in order to image seismically active faults or locate fracture systems in the subsurface.

2. BACKGROUND OF STUDY AREAS

2.1 Geology and geothermal activity

Hellisheidi is one of the high-temperature geothermal fields found in SW-Iceland, located in the southern part of the Hengill volcanic system (Björnsson et al., 1986). This active volcanic system is characterized by a 40-60 km long NNE-SSW trending fissure swarm with normal faults, fissures, frequent magma intrusions, and a central volcano (Figure 2).

The Hengill-Hellisheidi field (Figure 3) is expressed by numerous hydrothermal manifestations. Many explorations with different geoscientific disciplines have been carried out in this area. Resistivity surveys have revealed a large low-resistivity area, which can be interpreted as a layer dominated by smectite alterations representing temperatures between 100 and 200°C. This area is underlain by higher resistivity, which has been interpreted as formations including resistive high-temperature alteration such as chlorite and epidote (Árnason, 1993; Árnason et. al., 2000). The presence of chlorite and epidote indicates a temperature of 220-340°C. The Hellisheidi power plant is one of the biggest geothermal power plants in the world producing about 300 MW of electricity and hot water with a thermal capacity of 133 MW for district heating. Hellisheidi has two re-injection zones. The power company is required to inject all wastewater fluid back into the reservoir. The reason for this is twofold, firstly the wastewater must be injected below the groundwater table for environmental reasons and secondly it recharges the system. But this operation has three major challenges: The productivity of the injection decreases with time, the permeability depends on the temperature of the reinjected water and it can increase the level of seismicity.

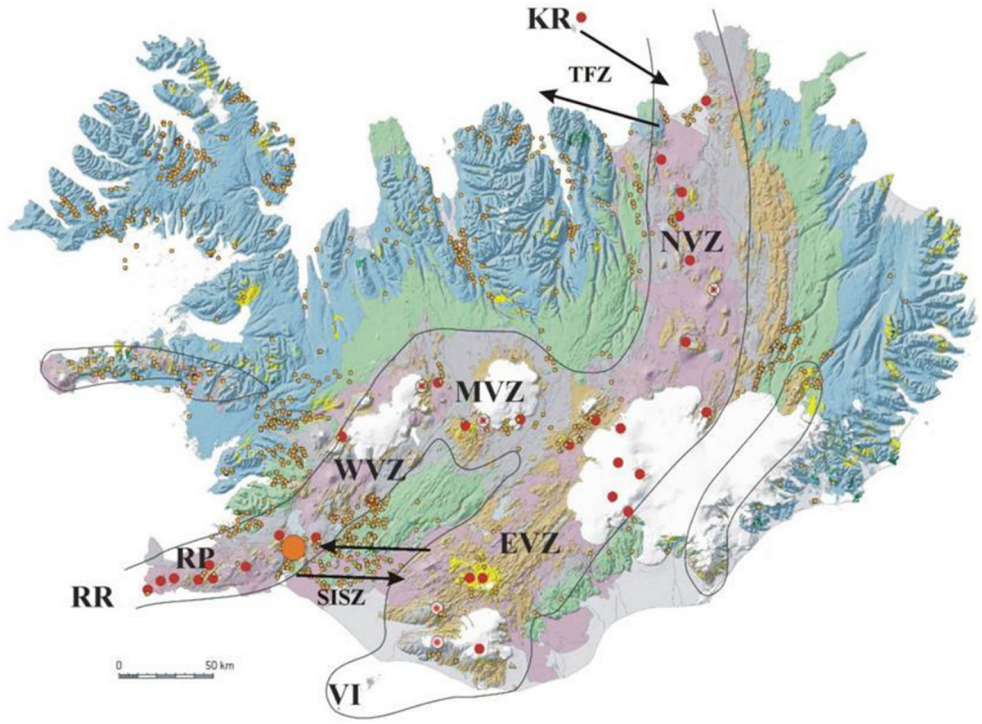

FIGURE 2: Geological map of Iceland showing the location of active volcanic zones and transform faults. RR = Reykjanes Ridge; RP = Reykjanes Peninsula; WVZ = Western Volcanic Zone; MVZ = Mid-Iceland Volcanic Zone; NVZ = Northern Volcanic Zone; EVZ = Eastern Volcanic Zone; VI Vestmanna Islands; SISZ = South Iceland Seismic Zone; TFZ = Tjörnes Fracture Zone. Red dots indicate high-temperature areas. Orange circle represents the approximate location of the Hengill volcanic system (Hardarson et al., 2010)

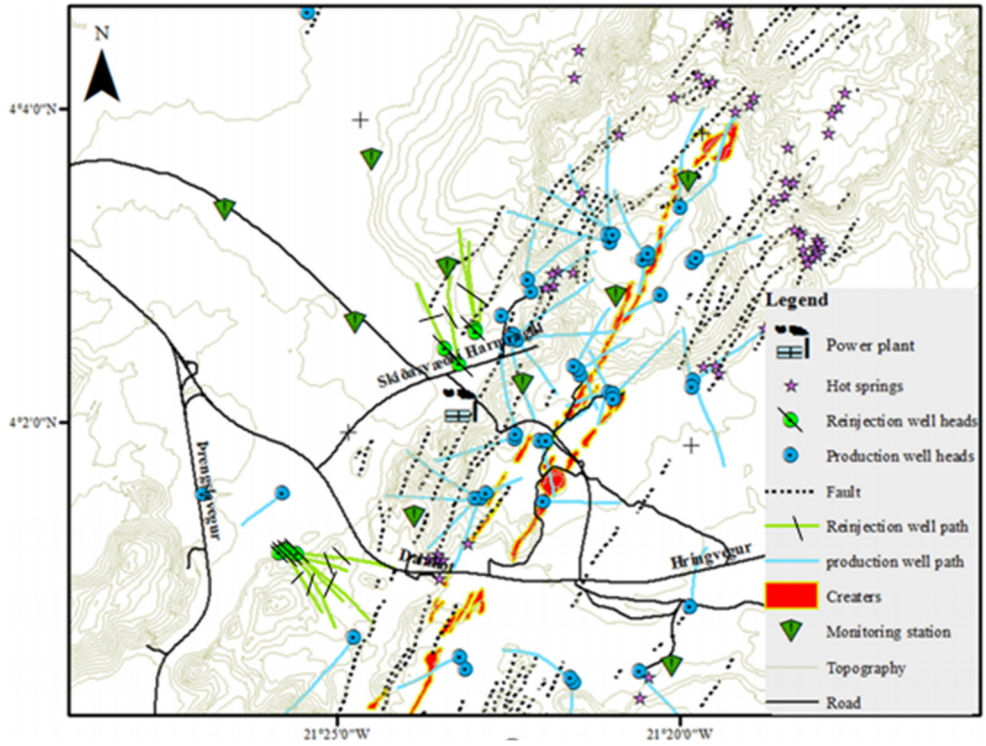

FIGURE 3: Topographical map of the Hellisheidi geothermal field with related faults, craters, surface manifestations, production wells, injection wells and seismic monitoring stations (Samaranayake, 2015)

2.2 Seismic activity

Mostly, the seismic activity in Hellisheidi is due to its location at a triple junction of a rather complex pattern of three tectonically active zones, the Reykjanes Peninsula, the Western Volcanic Zone and the South Iceland Seismic Zone (Figure 2). The two injection sites, Gráuhnjúkar and Húsmúli, in use at the Hellisheidi power plant have both been seismically active. After reinjection started at Gráuhnjúkar some events were recorded on the regional seismic network operated by the IMO, the largest magnitude registering at around 2.0 (Flóvenz et al., 2015). Seven injection wells have been drilled in the Húsmúli area. During the drilling of the last one in February 2011, intense induced seismicity repeatedly occurred, probably related to circulation loss (Ágústsson et al., 2015). It was monitored by a temporary local network operated by ÍSOR.

3. THEORY

3.1 Elastic seismic waves

Earthquakes are vibrations of the Earth caused by large releases of energy that accompany movements of the Earth´s crust and upper mantle, usually near tectonic plate boundaries, or associated with volcanic eruptions. There are different kinds of seismic waves such as body waves, which can travel through the Earth´s interior, and surface waves, which can only move along the surface. There are two kinds of body waves, called P waves and S waves. P waves involve compressional motion and volumetric changes as the wave disturbances passes through the continuum, but S waves involve shearing motions without volume change (Figure 4).

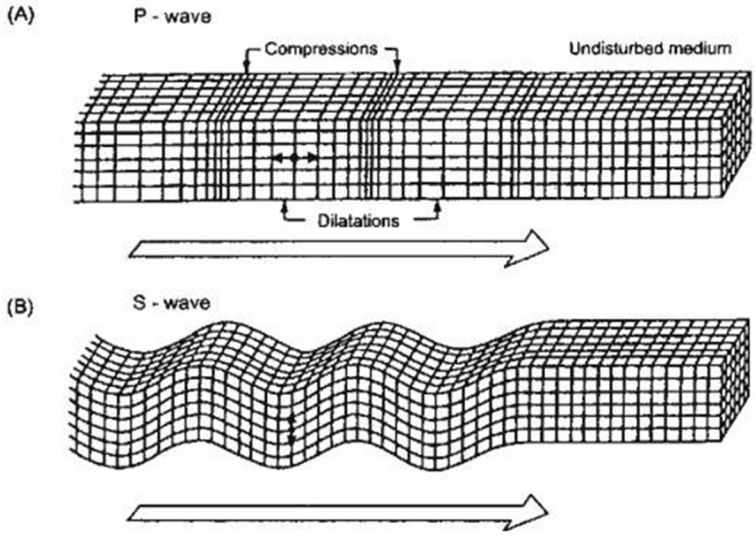

FIGURE 4: a) P wave travels through a medium by means of compression and dilation; b) S wave travels through a medium by means of shearing

To describe the behaviour of seismic waves we connect Hooke's law (linking stress and deformation) to Newton's law (connecting force and acceleration). Hooke´s law gives us the relationship between the stress and strain. In the case of a linear deformation in one direction (x axis) we get the following equation:

$$S_{xx} = \frac{\mathrm{E}\delta \mathrm{u}}{\delta x}$$
$$\text{or } S_{xx} = \mathrm{E}\, \varepsilon_{xx} \qquad (1)$$

giving:

$$\varepsilon_{xx} = \frac{\delta \mathrm{u}}{\delta x}$$

where E is called the Young´s modulus, $\frac{\delta \mathrm{u}}{\delta x}$ is the small displacement in the direction *x*, ε_{xx} is the strain and S_{xx} the stress.

For a body of three dimensions (Figure 5) this relationship is more complex because it takes into account both elongation along the *x* axis (ε_{xx}) and the contractions along the *y* and *z* axes (ε_{yy} and ε_{zz}) that are smaller than (ε_{xx}), and they are related by the same proportionality constant called Poisson´s ratio, $\sigma = \frac{\varepsilon_{yy}}{\varepsilon_{xx}}$. Hence we get:

$$S_{xx} = \frac{\mathrm{E}\delta u}{\delta x} \; -\sigma S_{xx} = \frac{\mathrm{E}\delta v}{\delta y} \; -\sigma S_{xx} = \frac{\mathrm{E}\delta w}{\delta z} \qquad (2)$$

with

$$\varepsilon_{xx} = \frac{\delta u}{\delta x} \; \varepsilon_{yy} = \frac{\delta v}{\delta y} \; \varepsilon_{zz} = \frac{\delta w}{\delta z}$$

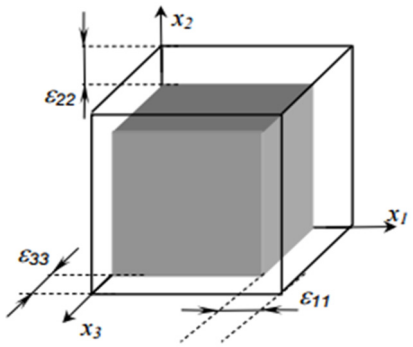

FIGURE 5: The relative change in volume of a cubic element subjected to a strain tensor ε

σ is between 0.2 and 0.3 for crystalline rocks and it is between 0.02 and 0.05 for sedimentary rocks. It can be expressed in terms of Young´s modulus E, and the Lamé constant λ, where:

$$\lambda = \frac{E\sigma}{(1+\sigma)(1-2\sigma)} \qquad (3)$$

Now, if we consider the relation between deformation and shear stress we get:

$$S_{xy} = S_{yx} = \mu\varepsilon_{xy} = \; \mu(\frac{\delta u}{\delta y} + \frac{\delta v}{\delta x}) \qquad (4)$$

μ is called shear modulus and varies between 0.1 and 0.7 Mbar for the most part of the rock. It can be expressed in terms of Young's modulus and Poisson's ratio:

$$\mu = \frac{E}{2(1+\sigma)} \qquad (5)$$

Using the Lamé constant λ defined in Equation 3 and from (Dix, 1952, p. 303-305) we write

$$S_{xx} = \frac{2\mu\delta u}{\delta x} + \lambda(\frac{\delta u}{\delta x} + \frac{\delta v}{\delta y} +) \qquad (6)$$

From the above Equations 1, 4 and 6 we get the Hooke´s relations that connect strains and stresses for solid ideals:

$$\begin{aligned} S_{xx} &= \frac{2\mu\delta u}{\delta x} + \lambda\theta \; S_{xy} = S_{yx} = \mu(\frac{\delta u}{\delta y} + \frac{\delta v}{\delta x}) \\ S_{yy} &= \frac{2\mu\delta v}{\delta y} + \lambda\theta \; S_{zx} = S_{xz} = \mu\left(\frac{\delta u}{\delta z} + \frac{\delta w}{\delta x}\right) \\ S_{xx} &= \frac{2\mu\delta w}{\delta z} + \lambda\theta \; S_{yz} = S_{zy} = \mu(\frac{\delta w}{\delta y} + \frac{\delta v}{\delta z}) \end{aligned} \qquad (7)$$

where $\theta = \varepsilon_{xx} + \varepsilon_{yy} + \varepsilon_{zz}$

Now we connect the Hooke´s relation (Equation 7) to Newton´ second law to get the velocities of the P wave and S wave (Equation 8):

$$\sum F = ma \qquad (8)$$

The large ∑ represents the vector sum of all the forces, the other side of the equation can be written as follows:

$$\rho dx dA \frac{d^2u}{dt^2} = ma \tag{9}$$

where ρ is the density and dA is the area of the section (Figure 6). Considering a small element dx is subjected to stress $S(x)$, the force applied is $S(x) \cdot dA$. Hence the net force is $[S(x+dx) - S(x)]dA$ which is also equal to ma (mass times acceleration). Using Equation 9 we get as follows:

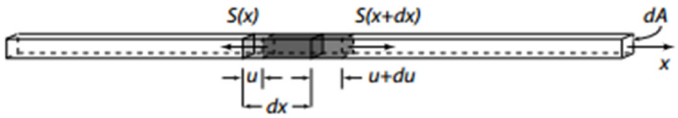

FIGURE 6: A small element *dx* subjected to a strain caused by a wave P

$$[S(x + dx) - S(x)]dA = \rho dx dA \frac{d^2u}{dt^2} \tag{10}$$

If $dx \rightarrow 0$, we can write as follows:

$$S(x + dx) - S(x) = \frac{dS}{dx} dx \tag{11}$$

Using Equation 1 and deriving we get:

$$\frac{dS}{dx} = \frac{Ed^2u}{dx^2}$$

so Equation 10 can be written as:

$$\frac{Ed^2u}{dx^2} dx dA = \rho dx dA \frac{d^2u}{dt^2} \tag{12}$$

After simplifying, we get:

$$\frac{d^2u}{dx^2} = \left(\frac{\rho}{E}\right) \frac{d^2u}{dt^2} \tag{13}$$

So the classic form of the wave equation in 1D is:

$$\frac{d^2u}{dx^2} = \left(\frac{1}{V^2}\right) \frac{d^2u}{dt^2} \tag{14}$$

where V is the wave velocity.

From Equations 13 and 14 we can deduce that:

$$V = \sqrt{\frac{E}{\rho}} \tag{15}$$

or, the wave velocity depends only on the Young's modulus and density.

If we consider the 3D case we get the solution for a compressional wave:

$$\frac{\delta^2\theta}{\delta x^2} + \frac{\delta^2\theta}{\delta y^2} + \frac{\delta^2\theta}{\delta z^2} = \frac{\rho}{\mu + \lambda} \frac{\delta^2\theta}{\delta t^2} \tag{16}$$

where $\frac{\rho}{\mu+\lambda} = \frac{\rho(1-2\sigma)(1+\sigma)}{E(1-\sigma)}$

λ is the second Lamé constant.

For a shear wave we get:

$$\frac{\delta^2\ \theta x}{\delta x^2} + \frac{\delta^2\ \theta x}{\delta y^2} + \frac{\delta^2\ \theta x}{\delta z^2} = \frac{\rho}{\mu}\frac{\delta^2\theta}{\delta t^2} \tag{17}$$

where $\theta x = \left(\frac{\delta w}{\delta y} - \frac{\delta v}{\delta z}\right)$.

Comparing Equations 16 and 17 with Equation 14 we get:

$$Vp = \sqrt{\frac{\lambda + 2\mu}{\rho}} \tag{18}$$

$$Vs = \sqrt{\frac{\mu}{\rho}} \tag{19}$$

From Equations 18 and 19, we can deduce the following:

- Vp is greater than Vs, meaning that the P wave arrives earlier than the S wave to recording stations on the surface.
- Since shear deformation is not possible in liquid ($\mu = 0$), shear waves do not propagate in liquid ($Vs = 0$).

3.2 Locating earthquakes

The main objective of observational seismology is to locate seismic sources. This involves determining two parameters, the hypocentre and the source origin-time. To solve these parameters requires the identification of seismic phases, measuring their arrival times, and knowledge of the velocity structure between the hypocentre and the seismic station. The data can either be processed with forward or inverse modelling procedures, which are used for interpreting seismic data as well as other geophysical data.

3.2.1 Hypocentre, epicentre and origin time

Hypocentre of an earthquake is the point where the rock starts to fracture, with the vibrating waves travelling away from this point in all directions. The epicentre is the point on land directly above the hypocentre. Origin time is the time when the earthquake started from hypocentre. It can be determined with a very simple graphical technique called a Wadati diagram (Figure 7). In this diagram the difference in arrival time for the S and P wave ($t_s - t_p$) is plotted against the absolute arrival time of the P wave. Since $t_s - t_p$ goes to zero at the hypocentre, a straight-line fit on the Wadati diagram gives the approximate origin time at the intercept with the P arrival time axis.

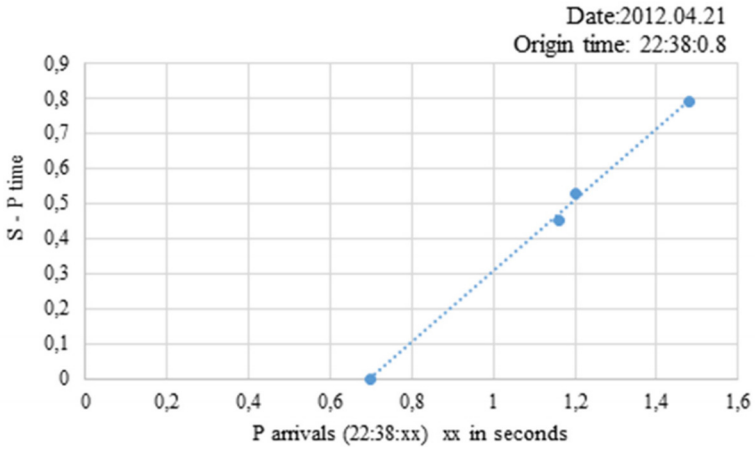

FIGURE 7: An example of a Wadati diagram used for determining the origin time; the intersection with the P wave arrival time axis gives the origin time (Samaranayake, 2015)

Once the origin time (OT) has been estimated, the epicentre distance for the i-th station can be estimated by tracking the travel time of the P wave and multiplying it by an estimate for the average P velocity α as follows:

$$D_i = (t_p^i - OT) \times \alpha \tag{20}$$

The epicentre must lie on a hemisphere of radius D_i centred on the i-th station. The epicentre should be located at the intersection of circles drawn for each station. The focal depth, D_{focal}, can be determined by taking the square root of the difference between the squares of propagation distance, D_i, and the distance along the surface to the epicentre, Δ, as follows:

$$D_{focal} = \sqrt{D_i^2 - \Delta^2} \tag{21}$$

3.2.2 Forward and inverse modelling

Forward models generate results that can be compared to observations. When we find a forward model that closely approximates the observations, we declare that the model sufficiently describes the earthquake location for the given model assumptions. Mathematically, we can think of this as a series of equations:

$$t_{ipredicted} = f(x_i, y_i, z_i, v) = t_{iobserved} \tag{22}$$

where v is the velocity, and *f* is a function which calculates the travel time, $t_{ipredicted}$, given (x_i, y_i, z_i) location of the earthquake and v.

If we have *n* stations at which we have actually measured arrival times, we can think of $t_{iobserved}$ as the *i*-th component of a data vector ***d*** that has *n* components, which we write as ***d*** = (t_1 , t_2,....., t_n). We can also consider the model parameters as a vector ***m*** that has four components for the spatial and temporal coordinates of the earthquake:

$$\boldsymbol{m} = (x, y, z, t_{ipredicted}) \tag{23}$$

Equation (22) can then be written as:

$$\boldsymbol{F}(\boldsymbol{m}) = \boldsymbol{d} \tag{24}$$

where ***F*** is a matrix called the data Kernel; x,y,z and t are the elements of the model vector ***m*** and ***d*** is a data vector where the output is the observation data $t_{iobservation}$.

If we could rearrange the term in Equation 24, such that we could divide **d** by some operator $\mathbf{F^{-1}}$ to give **m** directly, we would be solving an inverse problem. To develop how an inverse problem is done, consider an earthquake location in a homogenous material with velocity v. Then the *i-th* observed arrival time can be written as:

$$t_i = \frac{t_0 + \sqrt{(x_i - x)^2 + (y_i - y)^2 + (z_i - z)^2}}{v} \tag{25}$$

(i = 1,2,3,.....N)

where (x_i , y_i , z_i) = The location of the *i-th* station;
t_o = The common time origin;
(x,y,z) = The event location; and
N = = Number of observations.

F is an operator and nonlinear, so we must linearize the problem and establish an estimate of **m** and ***d***:

$$\boldsymbol{m = m_0 + \delta m} \tag{26}$$

$$\boldsymbol{\delta d = d - d_0} \tag{27}$$

where $\boldsymbol{\delta d, \delta m}$ are the incremental variation of the observed data and model parameter respectively.

Substituting both Equation 26 and 27 into Equation 24, and rewriting gives:

$$\boldsymbol{\delta d = d - d_0 = F(m_0 + \delta m) - F(m_0)} \tag{28}$$

Then to get linearization, we use only the first term of a truncated Taylor series as follows:

$$\boldsymbol{F(m_0 + \delta m) = F(m_0) + (\frac{\delta F(m)}{\delta m})_{m0} + O(m^2)} \tag{29}$$

So we can rewrite Equation 28 as:

$$\boldsymbol{\delta d = F(m_0 + \delta m) - F(m_0) = (\frac{\delta F(m)}{\delta m})_{m0} \delta m} \tag{30}$$

$$\boldsymbol{\delta d = G \delta m} \tag{31}$$

where $\boldsymbol{G = (\frac{\delta F(m)}{\delta m})_{m0}}$

Then we can rewrite Equation 31 as:

$$\boldsymbol{\Delta d = G\, \Delta m} \text{ or } \boldsymbol{d = G\, m} \tag{32}$$

This is the linearized form of the problem. If we have 4 stations we have $\boldsymbol{n = m}$ type problem and Gaussian elimination can be used to solve it. Once *δx, δy, δz* and *δt* are calculated, we can modify the parameters using Equation 27. This iterative process can be continued until $\boldsymbol{\Delta d}$ becomes acceptably small. This method is known as Geiger´s method. Its disadvantages are that the final model totally depends on the initial guess and the process does not guarantee convergence (Lay and Wallace, 1995).

Equation 32 relates a data vector of dimension *n* (number of observations) to a model vector of dimension *m* (number of model parameters). With many observations *(n>m)*, as in the case of earthquake location problems, we can obtain an overdetermined solution, which is the best fit to an average of the data.

3.3 Induced seismicity in geothermal fields

It is well known that geothermal systems are generally located in areas of tectonic activity, where earthquakes can take place. Evidence from earthquake studies indicate that the seismicity in geothermal areas is strongly influenced by the regional structures (Mulyadi, 1986). But earthquakes can also be induced by physical processes such as temperature, pressure, and stress changes associated with geothermal energy production; observable surface deformation associated with reservoir compaction around geothermal plants, and injection of liquid carbon dioxide at carbon sequestration plants (see Figure 8). Some of the major mechanisms of induced seismicity in geothermal environments are categorized as follows (Majer et al., 2007):

Pore pressure increase
Pore fluids are fluids that occupy pore spaces in soil or rock and play an important role in the stress field around earthquake faults. Increased fluid pressure in the pore of the rock or in the fault zone reduces the

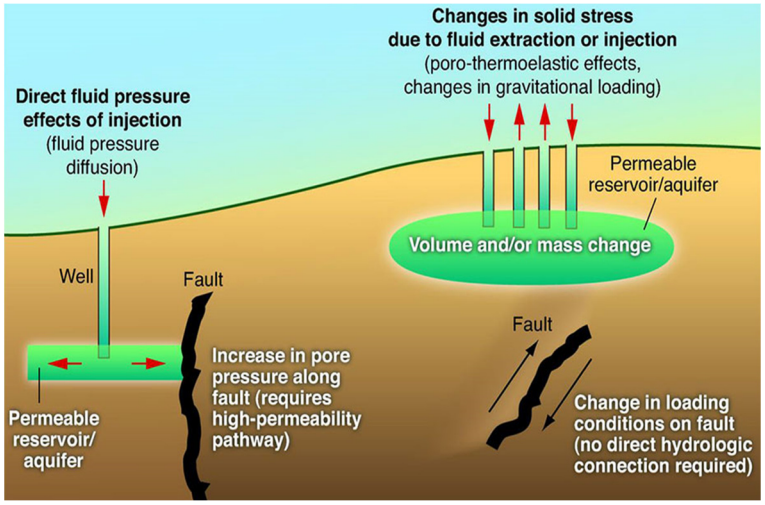

FIGURE 8: Schematic diagram of mechanisms for inducing earthquakes. Earthquakes may be induced by increasing the pore pressure acting on a fault (left) or by changing the shear and normal stress acting on the fault (right) (Ellsworth, 2013)

frictional strength of the fault or rock. Variation in fluid pressure may affect the timing of earthquakes (Miller, 1996).

Temperature decrease

Injection of cool fluids into the subsurface of geothermal areas allows cold fluid to interact with the hot rock and can cause contraction of fracture surfaces, in a process known as thermoelastic strain. Alternatively, cool fluid-hot rock interactions can create new fractures and seismicity directly related to thermal contraction of the rock matrix.

Volume change due to mass extraction and reinjection

As fluid is produced from (or injected into) an underground resource, the reservoir rock may compact or be stressed. These volume changes cause a perturbation in local stress conditions, which are already close to failure (geothermal systems are typically located within faulted regions under high states of stress). This situation can lead to seismic slip within or around the reservoir.

Chemical alteration of fracture surfaces

Injecting non-native fluid into the formation may cause geochemical alteration of fracture surfaces which cause a change in the coefficient of friction on those surfaces. This change of the coefficient of friction can cause microearthquakes.

4. DATA ACQUISITION AND PROCESSING

4.1 Setting up an earthquake monitoring network

To monitor earthquake activity in a particular area we need to install a seismic network, which has at least four stations, ideally in a Y-shaped configuration. The central station of the Y plays an important role to accurately get the depth of the earthquake and the three outer stations should be evenly spaced around the radius of the area of interest (Figure 9). A seismic monitoring system is made up of several parts: a seismograph, a power source, a data telemetry system, a data reception system, and data analysis software.

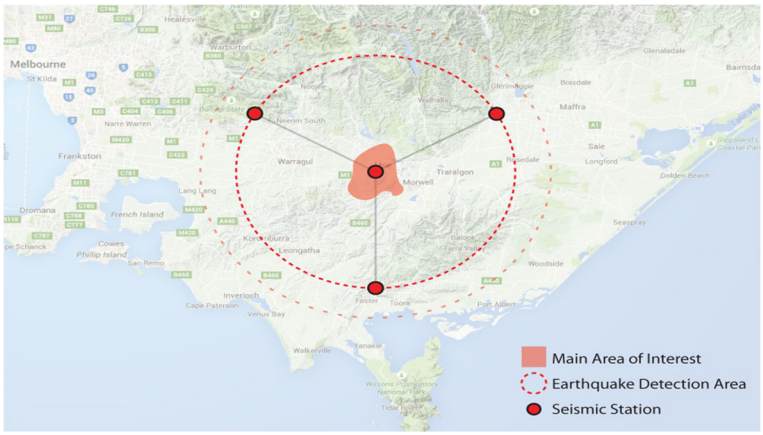

FIGURE 9: Installation of an earthquake monitoring network (Pascal, 2015)

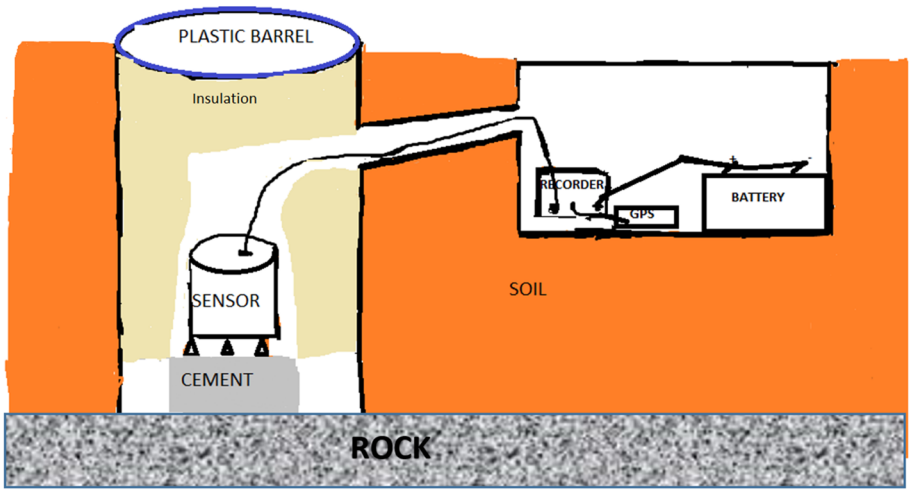

FIGURE 10: Seismometer installation

Seismographs are generally composed of two major components, a seismometer which is a sensor of ground motion and a recording system (Figure 10). Seismometers consist of three components, two of them measuring the horizontal motion along N-S and E-W and one along the vertical direction (Up-Down). Moreover, there are many different kinds of seismometers depending on the range of vibration frequencies that they can detect. Distinction is made between long period and short period seismometers which have become standards for global earthquake analyses, and broadband seismometers which can detect ground motions over a wide range of frequencies (Figure 11).

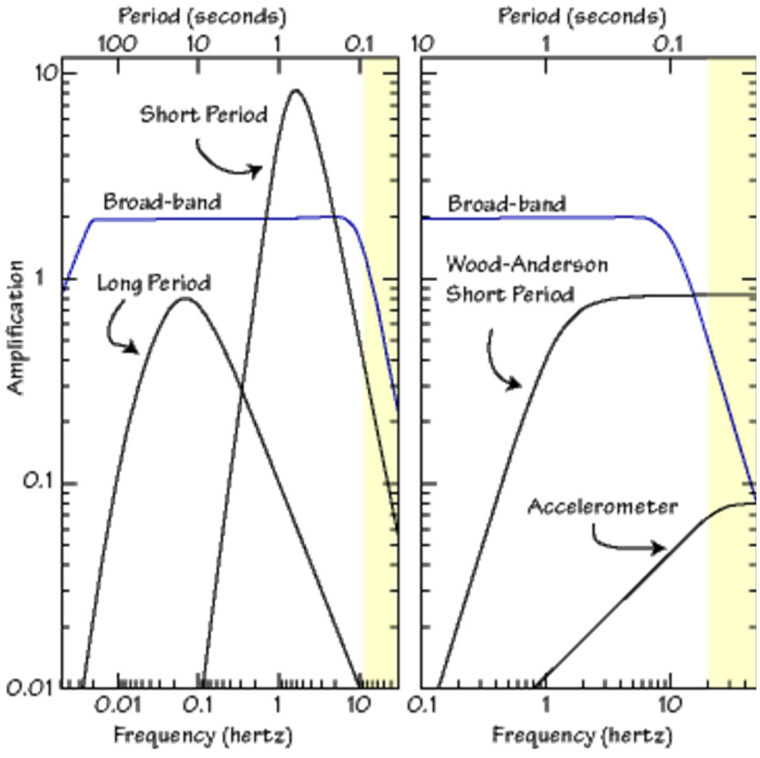

FIGURE 11: The broadband instrument senses most frequencies equally well; the long period and short period instruments are called “narrow” band and the yellow region is the low end of the frequency range audible to most humans (20 – 20000 Hz) (Department of Geoscience, 2016)

Usually the seismic station is deployed for a few months in the field, requiring a power source, such as a solar cell, a wind generator, direct connection to a landline and /or high capacity batteries. Obviously, the capacity of the batteries will determine how long the station will keep running. There are many ways in collecting data from the stations, either through a flash disk of high capacity set within the station, or to telemeter all the data continuously to the office.

Today there are more modern recorders using internet streaming to get the data sent in real time, and a software package can be set on the desktop computer to display the data on a screen, and to archive the data into manageable files. Then a data reception system can be set to analyse and to transfer the recorded data to the preliminary processing system. Detailed analysis of the earthquake is then undertaken using

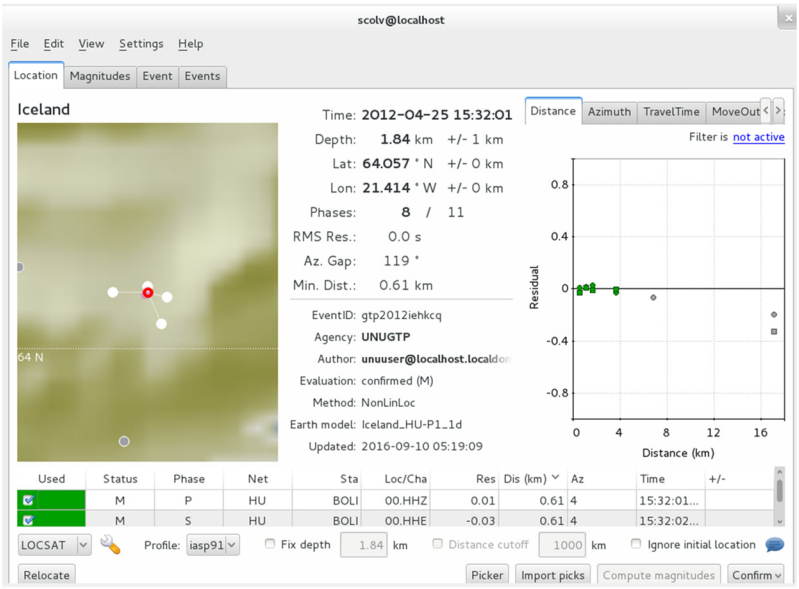

FIGURE 12: Front page view of the SeisComP3 software

analysis and modelling software and the earthquake information stored into a database to form a permanent historical record of seismic activity. In this project, a software called SeisComp3 (2016) (Seismological Communication Processor) is used, which was developed for the GEOPHON program, and is maintained by GEOPHON software development group at GFZ Potsdam. SeisComp3 can be download for free from the internet (*www.seiscomp3.com*) and consists of acquisition, picking and analysing facilities and it is able to accurately determine an earthquake´s location as well as its magnitude. Figure 12 shows the front page view of the software. The different steps used to process data in this project are as following:

- Enter the location of the interest area and the origin time through **Location** window;
- Go to **Picker** window;
- Change band pass filter to enhance the signal, in this case 4-50 Hz bandpass filter is used;
- Pick P and S wave arrival times for all the stations (Figure 13);
- Return to the main window and select nonlinear location method and velocity model to relocate the earthquake (Figure 14).

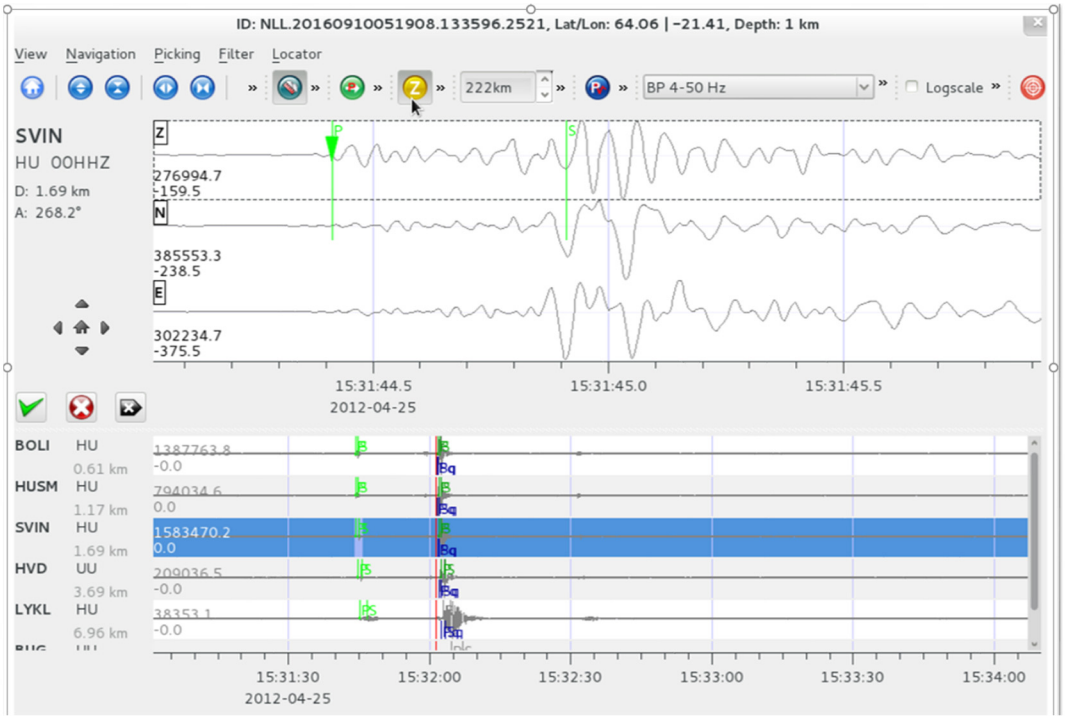

FIGURE 13: Picker window in the SeisComP3 software showing P and S waves from an event in Hellisheidi

4.2 Seismic noise

As for any measurement of physical properties, seismic data contains undesired components of ground motion called seismic noise. It is caused by several sources, which can be divided into coherent noise or incoherent noise.

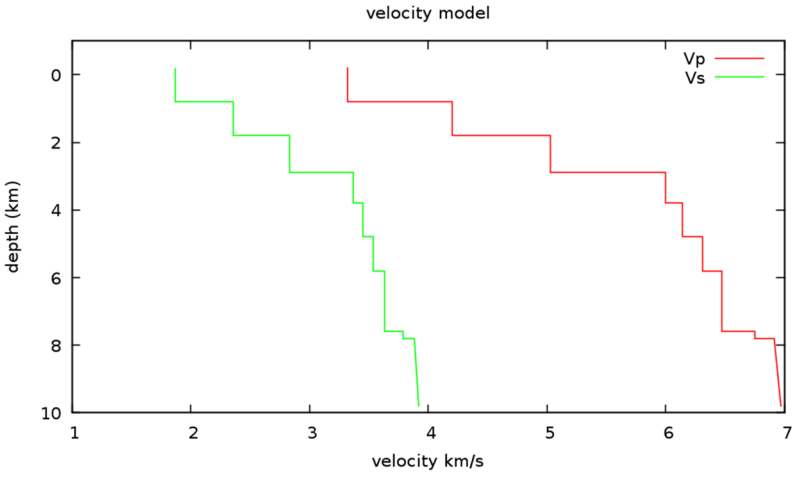

FIGURE 14: Velocity model used for the seismic data processing (Vogfjörd and Hjaltadóttir, 2007)

- Coherent noise includes surfaces waves, reflections or reflected refractions from near surface structures such as fault planes or buried stream channels, refractions carried by high-velocity stringers, noise caused by vehicular traffic or farm tractors, multiples, etc. All of the preceding except multiples travel essentially horizontally.

There are several techniques to reduce the noise and to enhance the seismic signal such as:

- Frequency filtering can be used to advantage (very low frequency components may be filtered out during the initial recording provided the low frequencies are sufficiently separated from the reflection frequencies).
- Protection from environmental noise such as temperature fluctuation, turbulent air flow around walls and human activity at the station.

5. RESULTS AND DISCUSSION

5.1 Hellisheidi area

Hellisheidi area has two reinjection zones, Gráuhnjúkar and Húsmúli. Gráuhnjúkar area is situated on the southern edge of the field. The temperature at depth in this area is higher than 300°C and could be ideal for production. Húsmúli is located in the northwestern part of the field. Seven reinjection wells have been drilled there, the last one in February 2011. Several earthquakes were recorded on a local network during the drilling of the injection wells. They seemed to be related to loss in drilling fluid during drilling operations (Ágústsson et al., 2015). When the reinjection of the waste water of the Hellisheidi power plant started in September 2011, a large number of induced earthquakes were recorded in the Húsmúli area by the Icelandic Meteorological office (IMO). During the period from 2011 to 2012 thousands of earthquakes were located (Figure 15). Four earthquakes with magnitude above 3.0 were observed, and felt in neighbouring

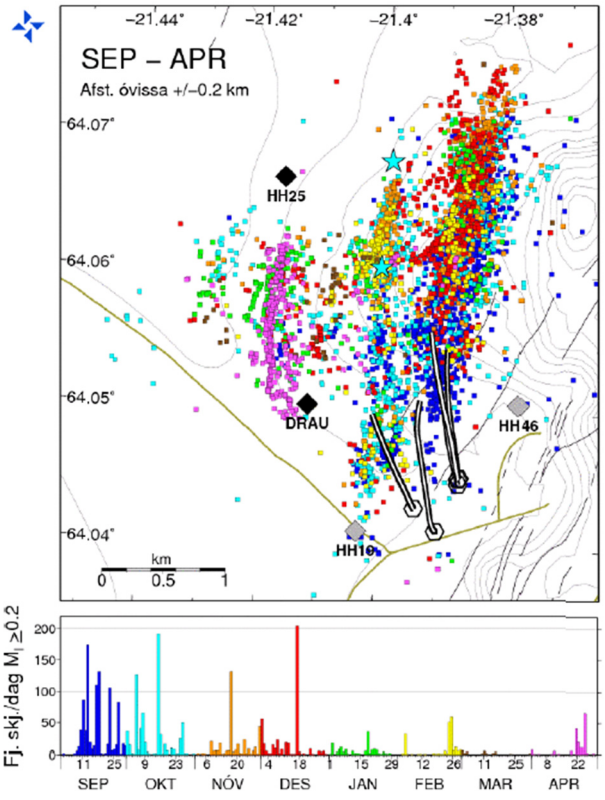

FIGURE 15: Induced seismicity in the Húsmúli area during 2011-2012 (Bessason et al., 2012)

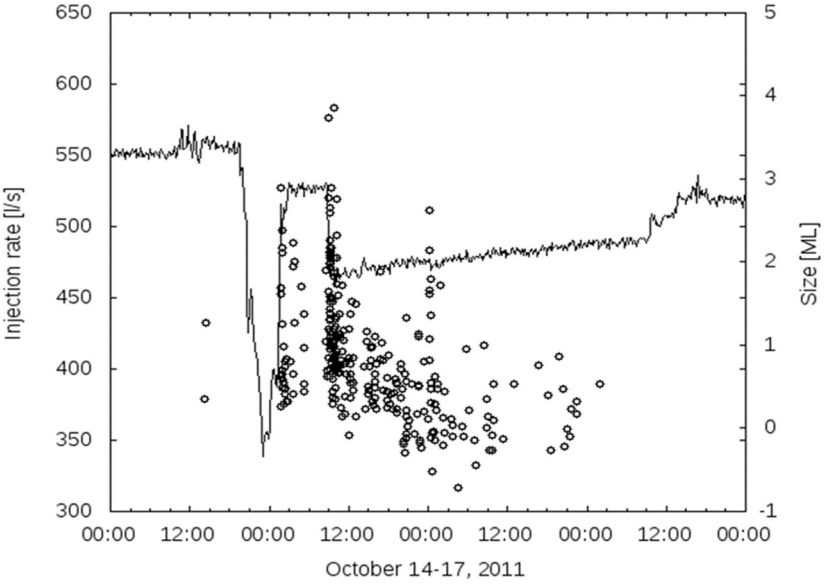

FIGURE 16: Relationship between injection and seismicity (Kristjánsdóttir, S., personal communication)

municipalities, closest of which is ~ 8 km from the epicentre. Over time the built-up stress in the area was released, leading to a decrease in the seismicity. A link has been found between rapid changes in the reinjection rate and seismicity (Figure 16), therefore injection rate is kept as steady as possible in order to minimize induced seismic activity. Figure 15 also shows that the seismicity is characterized by several swarms, which delineate north-south striking faults, with the activity moving from east to west as time progresses.

In this report, data from of a swarm from April 25th, 2012, was analysed using the SeiscomP3 seismological software, developed by Helmholtz Centre Potsdam, GFZ German Research Centre for Geosciences in collaboration with GEMPA GmbH (2016). In all, 168 earthquakes were picked and located. Figure 17 shows the locations of the earthquakes on different views and the distributions of the magnitude of the recorded events. The detection threshold of the network is around 0.5. This means that events with magnitude below 0.5 are not all detected. A map view of the swarm shows a concentration of earthquakes in the Húsmúli area. They seem to delineate a N-S striking fault, which is vertically dipping (see cross-section). The activity is limited to a depth of 1.5-2.5 km although the uncertainty could be up to ± 1.0 km.

5.2 Overview and discussion on micro-seismic survey in Hanle Gaggade

The Republic of Djibouti is one of the East African countries, which has an exceptional geodynamic situation. It is located at the triple junction of the Red Sea, Gulf of Aden, and East African rifts where volcanic and tectonic activity has been taking place for 30 My (Jalludin, 2014). A recent reconnaissance study done by JICA (Japan International Cooperation Agency) in the whole region of the Republic of Djibouti, identified thirteen potential geothermal fields. Our discussion focuses on a microseismic survey undertaken in the Hanle–Gaggade area (one of the potential geothermal fields) from January 29, 2016 until May 3, 2016.

5.2.1 Geology of Hanle Gaggade

Hanle-Gaggade is located in the south-western region of the country where stratoid basalts circumscribe a succession of high plateaus and sedimentary plains between Lake Abhe and Lake Asal (Figure 18). Within this wide zone, fumaroles and hot springs are identified in the Lake Abhe area, the Galafi plain, on the eastern side of the rhyolitic Baba Alou Mountain and along the northern border of the Gaggade plain. Temperatures of the hot springs can exceed 60°C (Jalludin, 2014).

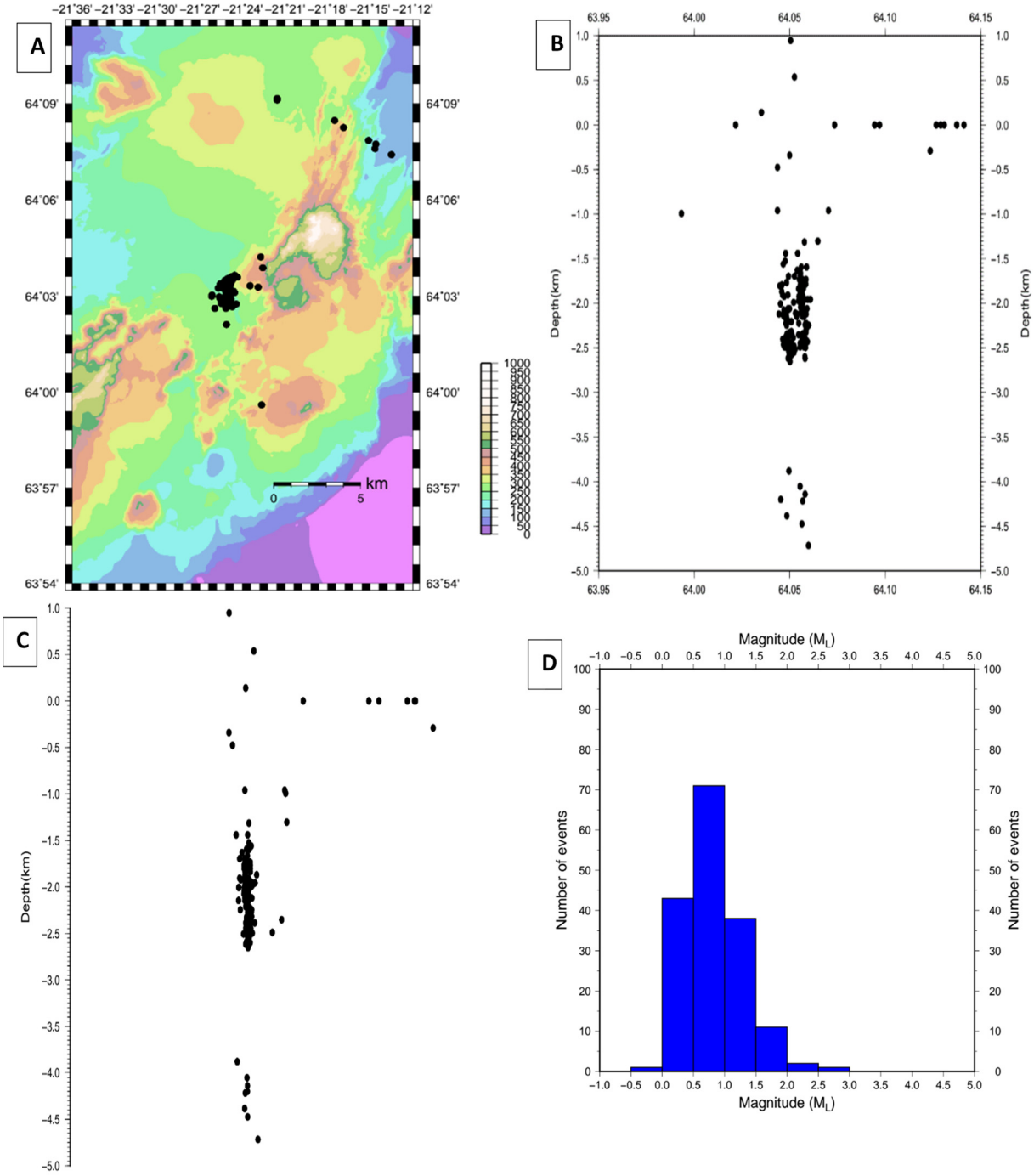

FIGURE 17: Location of the seismic activities a) on top of a topographic map (view from above); b) view from east; c) view from south; and d) magnitude distribution of the recorded events

Recently, the new Djiboutian Office of Geothermal Development (ODDEG) with support from JICA carried out a huge geophysical survey combining several methods such as identifying geothermal fluid movement and the brittle-ductile transition zone, gravity survey for consideration of geological structure in connection with geothermal reservoir system, and MT/TDEM survey to study the underground resistivity structure of the target field. An environmental and social impact assessment is ongoing in parallel. The final report was finalized in July 2016 in order to trigger the next step: the test well drillings.

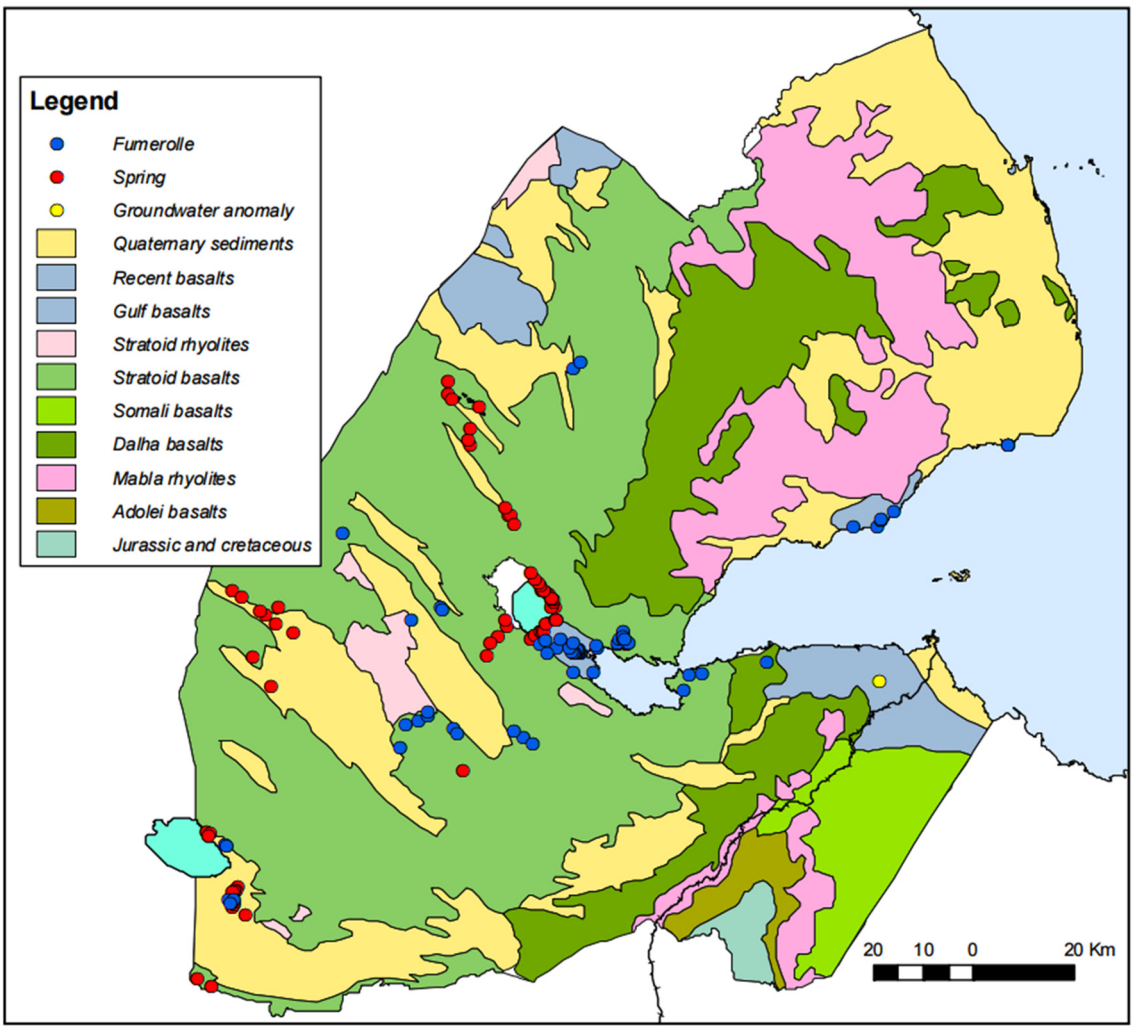

FIGURE 18: Geology and hydrothermal activity in the Republic of Djibouti (Jalludin, 2014)

5.2.2 Micro-seismic surveys

Following the MT/TEM and gravity surveys, a microseismic survey was conducted in August 2016 by ODDEG, covering approximately the same area as the geophysical surveys (MT/TEM, gravity). Velocity-type seismometers consisting of 3 components (N-S, E-W, Up-Down) were installed and collected data for about three months at five different locations. The purpose of this micro-earthquake survey was to understand areas with signs of geothermal activity, and to confirm fault structures and the positions of fault systems.

Figure 19 shows the locations of earthquakes recorded in the study area during the observation period. Most events are located on the lava plateau. A swarm of earthquakes was concentrated on the northwest part of the study area where the rhyolites are more dominant than the lower basalt rock but they were scattered outside of the station network. Distribution of epicentres seems to be concentrated near some faults, which could mean that those faults are active. More accurate locations, such as with relative relocation methods, are necessary to confirm this. In light of the recorded seismic activity, a local seismic network is recommended to monitor microseismic activity in this area during the exploitation of the geothermal field.

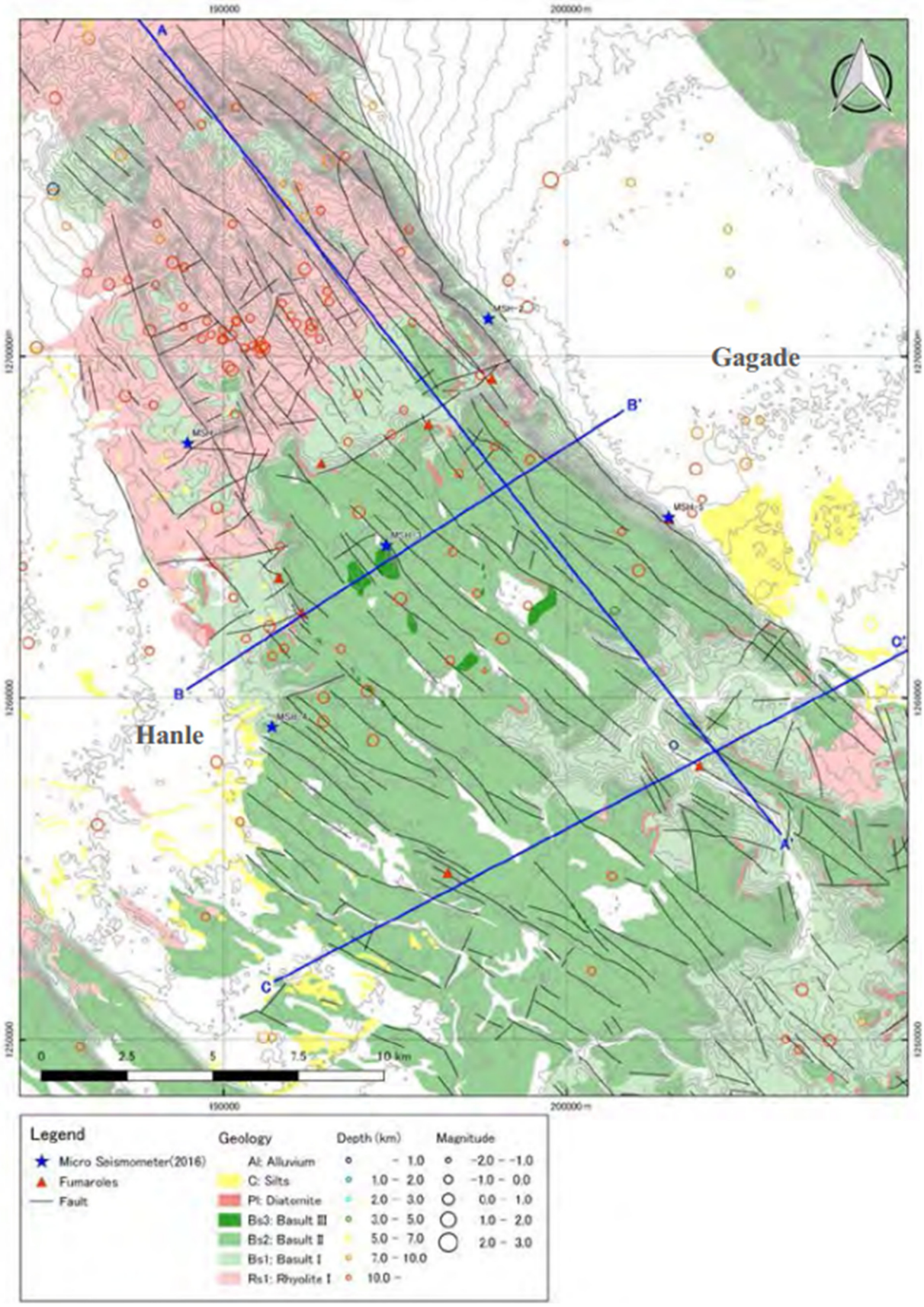

FIGURE 19: Distribution of epicentres in the study area (ODDEG, 2016)

6. CONCLUSION

It is important to minimize negative impacts of induced seismicity and increase the positive aspects for the sustainable use of resources. It is observed, also from microearthquake surveys done in Hanle Gaggade area, that this technique is a helpful tool in the exploration of a geothermal field in order to locate the brittle ductile zone and to map the active faults in a geothermal system. To be able to do that a continuous dataset recording both natural and induced seismicity needs to be analysed.

ACKNOWLEDGEMENTS

First and foremost, I am grateful to Mr. Abdou-Houmed and Mr. Lúdvík S. Georgsson for giving me the opportunity to participate in the UNU Geothermal Training Programme in Iceland.

I am grateful to my supervisor Ms. Sigrídur Kristjánsdóttir. I am deeply indebted to her whole-hearted supervision to me during the project period. Her valuable suggestions and guidelines helped me a lot to prepare the report in a well-organized manner.

I would like to thank Mr. Gylfi Páll Hersir and Ms. Ásdís Benediktsdóttir for their constant advice, encouragement and their helping hand to complete my report successfully. I wish also to thank Ingimar, Frída, Thórhildur and Markús, the staff of UNU-GTP who rendered their help during this training programme.

I would also like to thank all the 2016 UNU-fellows for their friendship and fellow feeling.

Finally, I would like to express my deepest gratitude to almighty Allah for giving me the strength and the composure to complete this report.

REFERENCES

Ágústsson, K., Kristjánsdóttir, S., Flóvenz, Ó.G., Gudmundsson, Ó., 2015: Induced seismic activity during drill of injection well at the Hellisheidi power plant, SW Iceland. *Proceedings of the World Geothermal Congress 2015, Melbourne, Australia,* 10 pp.

Árnason, K., 1993*: Relation between resistivity and geothermal activity in basaltic rocks*. English translation of a chapter in: Geothermal activity at the Ölkelduháls field, resistivity soundings in 1991 and 1992. Orkustofnun, Reykjavík, report OS-93037/JHD-10 (in Icelandic), 82 pp.

Árnason, K., Karlsdóttir, R., Eysteinsson, H., Flóvenz, Ó.G., and Gudlaugsson, S.Th., 2000: The resistivity structure of high-temperature geothermal systems in Iceland. *Proceedings of the World Geothermal Congress 2000, Kyushu-Tohoku, Japan*, 923-928.

Bessason, B., Ólafsson, E.H., Gunnarsson, G., Flóvenz, Ó.G., Jakobsdóttir, S.S., Björnsson, S., and Árnadóttir, Th., 2012: *Working procedures due to induced seismicity in geothermal systems*. Reykjavík Energy, Reykjavík, internal report (in Icelandic), 10 pp.

Björnsson, A., Hersir, G.P., and Björnsson, G., 1986: The Hengill high-temperature area, SW-Iceland: Regional geophysical survey. *Geothermal Resources Council, Transactions, 10,* 205-210.

Department of Geosciences, 2016: *Wave, seismograms and seismometers.* PennState, College of Earth and Mineral Scences, Department of Geosciences, website: *eqseis.geosc.psu.edu/~cammon/ HTML/Classes/IntroQuakes/Notes/seismometers.html#seismic_networks.*

Dix, C.H., 1952: *Seismic prospecting for oil.* Harper & Brothers, NY, 414 pp.

Ellsworth, W.L., 2013: Injection-induced earthquakes. *Science, 341-6142*.

Flóvenz, Ó.G., Ágústsson, K., Gudnason, E.Á., Kristjánsdóttir, S., 2015: Reinjection and induced seismicity in geothermal fields in Iceland. *Proceedings of the World Geothermal Congress 2015, Melbourne, Australia,* 15 pp.

Foulger, G.R., and Julien, B.R., 2009: *Applied microearthquake techniques for geothermal resource development.* Durham University, Durham, UK, website: *community.dur.ac.uk.*

Geothermal Education Office, 2007: *Geothermal reservoir*. Geothermal Education Office, website: *geothermaleducation.org/GEOpresentation/sld012.htm.*

Hardarson B.S., Einarsson, G.M., Gunnarsson, G., Helgadóttir H.M., Franzson, H., Árnason K., Ágústsson, K. and Gunnlaugsson E., 2010: Geothermal Reinjection at the Hengill Triple Junction, SW Iceland. *Proceedings of the World Geothermal Congress 2010, Bali, Indonesia,* 7 pp.

Jalludin. M., 2014: State of knowledge of the geothermal provinces of the Republic of Djibouti. *Paper presented at „Short Course IX on Exploration for Geothermal Resources", organized by UNU-GTP, GDC and KenGen in Lake Bogoria and Lake Naivasha, Kenya*, UNU-GTP SC-19, 17 pp.

Lay, T., and Wallace, T.C., 1995: *Modern global seismology*. Academic Press, San Diego, CA, 521 pp.

Majer, E.L., Baria, R., Stark, M., Oates, S., Bommer, J., Smith, B., and Asanuma, H., 2007: Induced seismicity associated with enhanced geothermal systems. *Geothermics, 36-3,* 185-222.

Miller, S.A., 1996: Fluid-mediated influence of adjacent thrusting on the seismic cycle at Parkfield. *Nature, 382,* 799-802.

Mulyadi, 1986: *Applications of resistivity methods and micro-earthquake monitoring in geothermal exploration.* UNU-GTP, Iceland, report 6, 52 pp.

ODDEG, 2016: *Micro-seismic survey in Hanle Gaggade*. ODDEG – Djiboutian Development Office of Geothermal Energy, Workshop, Djibouti, August.

Pascale, A., 2015*: Setting up an earthquake monitoring network.* Seismology Research Centre, website: *www.src.com.au.*

Samaranyake, S.A., 2015: Seismic monitoring of geothermal fields: a case study of Hellisheidi geothermal field, Iceland. Report 32 in: *Geothermal training in Iceland 2015*. UNU-GTP, Iceland, 727-754.

SeisComp3, 2016: *Seiscomp3 software*. Seismological Communication Processor, website: *www.seiscomp3.org/.*

Vogfjörd, K.S., and Hjaltadóttir, S., 2007: *Mapping of seismic activity at Hverahlíd in Hellisheidi in February 2006*. Icelandic Meteorological Office, Reykjavík, report 07010 (in Icelandic), 20 pp.

Wanjohi, A.W., 2007: Monitoring of micro earthquakes and acoustic emissions within the Hengill-Hellisheidi geothermal reservoirs, June-August 2007. Report 23 in: *Geothermal training in Iceland 2007.* UNU-GTP, Iceland, 555-580.

APPENDIX I: Temporary seismic networks operated in the Hellisheidi area

Number	Station name	Latitude	Longitude	Height
1	BIT	64.05730	-21.25770	0.390
2	GUD	64.01973	-21.18845	0.104
3	HVH	64.00967	-21.33558	0.380
4	LHA	64.02406	-21.04883	0.119
5	IND	64.06153	-21.33585	0.470
6	SHR	64.02401	-21.50160	0.367
7	SKD	64.10792	-21.29883	0.344
8	BJA	63.94590	-21.30258	0.057
9	HEI	64.19978	-21.23603	0.162
10	KAS	64.02290	-21.85200	0.108
11	KRO	64.09806	-21.11976	0.147
12	SAN	64.05602	-21.57013	0.208
13	SOL	63.96230	-20.94357	0.030
14	VOS	63.85279	-21.70357	0.008
15	BUG	63.90450	-21.43760	0.034
16	ENG	64.08783	-21.41047	0.267
17	GEI	63.94818	-21.53068	0.278
18	HVD	64.02451	-21.39945	0.328
19	HVV	64.11147	-21.21532	0.181
20	LHL	63.97915	-21.83195	0.192
21	LME	63.97420	-21.42910	0.255
22	LSK	64.03495	-21.29603	0.367
23	NUP	63.99884	-21.25361	0.300
24	SEL	64.13364	-21.23823	0.169
25	SOG	63.99224	-21.14963	0.065
26	SVH	63.87788	-21.55152	0.150
27	TRH	64.06075	-21.17984	0.342

APPENDIX II: Seismic events recorded during April 24, 2012

Latitude	Longitude	Depth (km)	Origin time	Magnitude
64.05039	-21.43574	-0.948	00:01:01.374	0.53
64.05461	-21.38147	2.352	00:04:04.737	0.5
64.05602	-21.41534	1.973	00:07:14.009	0.34
64.05461	-21.41923	1.836	00:09:31.808	0.53
64.04987	-21.43610	0.341	00:12:04.940	0.3
64.05769	-21.41609	2.412	00:14:48.368	0.96
64.05681	-21.41802	2.343	00:15:52.870	0.77
64.03510	-21.41875	-0.141	00:21:21.584	0.51
64.04829	-21.42029	1.767	00:25:21.466	0.28
64.05839	-21.41454	2.326	00:27:24.682	0.82
63.99327	-21.37744	0.994	00:28:50.351	0.66
64.05479	-21.42367	1.922	00:30:42.845	0.14
64.05707	-21.41623	2.352	00:32:12.078	0.69
64.05532	-21.41688	1.973	00:33:59.260	0.5
64.06463	-21.37629	1.303	00:38:24.406	0.39
64.05496	-21.41846	1.836	00:44:58.868	0.46
64.05250	-21.41021	-0.536	00:56:22.544	0.15
64.05602	-21.41775	1.595	01:07:05.944	0.45
64.05154	-21.41716	2.480	01:08:13.668	0.74
64.05075	-21.41327	2.317	01:11:08.397	0.77
64.05224	-21.41521	2.549	01:15:33.498	1.41
64.05136	-21.41554	2.566	01:18:59.361	0.84
64.05224	-21.41722	2.480	01:23:07.437	1.45
64.05136	-21.41554	2.480	01:37:45.620	1.7
64.05066	-21.41507	2.446	01:57:23.877	0.99
64.04899	-21.41875	2.077	02:01:07.916	0.5
64.04978	-21.41781	2.326	02:02:59.213	1.15
64.05110	-21.41571	2.352	02:04:05.690	1.04
64.05892	-21.41258	2.274	02:12:21.010	1.37
64.05277	-21.41405	2.515	02:15:03.533	2.07
64.05769	-21.41528	1.312	02:16:56.625	1.22
64.05804	-21.41370	2.395	02:19:09.647	1.81
64.05356	-21.41673	2.145	02:42:00.416	0.93
64.05083	-21.41589	2.205	02:45:43.733	1.14
64.04635	-21.41812	2.128	02:49:26.701	0.37
64.04732	-21.41479	2.463	02:50:06.308	1.13
64.04723	-21.41538	2.489	02:53:45.857	0.54
64.04864	-21.41791	2.180	02:55:21.177	0.49
64.04662	-21.41392	2.463	02:56:40.107	1.4
64.05409	-21.42843	1.441	03:07:17.681	0.84
64.04354	-21.43233	0.478	03:10:22.043	0.33
64.05532	-21.41608	1.802	03:14:58.730	0.95
64.04952	-21.42723	3.881	03:15:56.180	1.49

Latitude	Longitude	Depth (km)	Origin time	Magnitude
64.05496	-21.41846	1.733	03:17:53.046	0.89
64.04697	-21.41957	2.120	03:19:55.486	1.24
64.05540	-21.41870	2.446	03:22:15.201	1.06
64.05989	-21.41326	2.248	03:29:13.046	1.22
64.05532	-21.41769	1.939	03:31:04.326	0.64
64.04934	-21.41878	1.698	03:35:43.417	0.53
64.05286	-21.41667	2.111	03:44:31.154	0.66
64.05066	-21.41668	2.584	03:48:45.482	1.05
64.05013	-21.41623	2.652	03:50:12.372	0.8
64.04960	-21.41860	2.618	03:53:05.099	0.43
64.04837	-21.41327	2.446	03:57:38.389	1.37
64.05637	-21.42582	2.008	04:00:26.671	0.24
64.04618	-21.42493	1.905	04:05:15.367	0.84
64.04829	-21.42592	2.145	04:05:47.962	0.87
64.04512	-21.42002	2.008	04:06:57.909	0.39
64.04433	-21.41212	2.120	04:10:54.016	1.58
64.04960	-21.41699	2.549	04:17:02.186	1.15
64.04996	-21.41702	2.498	04:19:18.711	0.97
64.05628	-21.41717	2.412	04:53:07.633	1.21
64.05365	-21.41533	2.120	05:01:50.572	1.5
64.04996	-21.41582	2.343	05:05:45.791	1.1
64.04829	-21.42431	2.248	05:08:21.832	1.06
64.04908	-21.41735	2.618	05:09:54.441	1.29
64.05804	-21.41491	2.618	05:13:24.325	1.24
64.05470	-21.41462	2.223	05:16:05.877	1.32
64.04969	-21.41800	2.592	05:21:31.048	0.47
64.04785	-21.41363	2.377	05:29:13.339	1.3
64.05532	-21.41929	1.870	05:30:45.356	0.59
64.04688	-21.41615	2.077	05:32:50.992	0.63
64.05787	-21.41409	2.601	05:35:06.343	1.01
64.04802	-21.41525	2.395	05:40:34.748	1.34
64.04855	-21.41569	2.343	05:56:54.411	2.75
64.04837	-21.41447	2.498	06:00:15.192	0.97
64.05857	-21.41656	2.120	06:03:42.073	1.52
64.05734	-21.41726	2.120	06:06:55.391	1.46
64.05839	-21.41695	2.223	06:08:08.427	1.5
64.04916	-21.41836	2.059	06:12:39.273	0.54
64.06077	-21.40892	1.956	06:16:12.227	0.2
64.05180	-21.40935	2.386	06:18:06.591	1.19
64.05602	-21.41936	2.077	06:21:22.675	0.59
64.04987	-21.41842	2.059	06:28:16.428	0.28
64.05532	-21.39117	2.489	06:29:58.087	0.54
64.04354	-21.41948	0.959	06:33:12.016	0.49
64.04899	-21.41875	2.386	06:34:25.449	0.4

Latitude	Longitude	Depth (km)	Origin time	Magnitude
64.04635	-21.41812	2.403	06:37:56.728	0.27
64.09447	-21.18683	0	06:40:05.878	0.6
64.13749	-21.28121	0	06:41:31.530	0.45
64.02166	-21.60935	0	06:55:53.353	0.47
64.09705	-21.17714	0	06:57:24.259	0.87
64.07349	-21.17723	0	06:59:33.385	0.75
64.04839	-21.41968	4.384	07:01:34.142	0.73
64.04952	-21.42080	2.506	07:05:09.319	0.28
64.05672	-21.41942	1.733	07:08:31.953	0.02
64.05250	-21.41985	1.698	07:09:58.986	0.57
64.05532	-21.41849	1.733	07:17:45.620	0.52
64.04864	-21.41872	2.214	07:26:29.942	0.49
64.05830	-21.41594	1.784	07:34:24.254	0.28
64.05690	-21.41582	2.059	07:38:14.499	0.8
64.07026	-21.37838	0.959	07:40:35.424	0.21
64.04653	-21.41291	1.561	07:45:35.488	0.58
64.04591	-21.41788	1.793	07:47:22.870	0.93
64.05567	-21.41691	1.664	07:51:06.623	0.25
64.05532	-21.42492	1.698	07:53:40.586	0.59
64.05690	-21.41903	1.922	07:54:43.199	0.72
64.05198	-21.41218	1.991	07:57:15.357	0.46
64.04899	-21.41634	1.905	08:01:47.858	0.29
64.05672	-21.41540	1.802	08:02:50.265	0.45
64.05936	-21.41201	1.956	08:04:40.308	0.22
64.05532	-21.42010	1.905	08:18:28.517	0.22
64.04477	-21.41677	1.802	08:28:13.650	-0.44
64.04811	-21.41425	2.231	08:35:15.217	0.54
64.04758	-21.41541	1.527	08:37:33.244	0.49
64.04582	-21.40723	1.870	08:41:49.805	0.52
64.05883	-21.41237	2.248	08:44:09.388	0.95
64.05461	-21.41923	1.973	08:58:40.357	0.5
64.05602	-21.42016	1.802	09:04:36.952	0.36
64.05602	-21.41936	2.111	09:17:28.010	0.4
64.05602	-21.41855	2.042	09:28:36.118	0.88
64.05813	-21.42034	2.077	09:32:39.830	0.32
64.04688	-21.41696	2.145	09:34:10.639	0.5
64.04705	-21.41496	1.922	09:35:33.125	0.44
64.04776	-21.41663	1.441	09:40:26.166	0.27
64.05760	-21.41588	2.334	09:43:27.848	0.59
64.05637	-21.41778	2.111	09:47:44.274	0.58
64.05848	-21.41234	2.317	09:51:32.478	0.9
64.05672	-21.41942	2.145	09:54:51.399	0.49
64.05567	-21.42013	2.042	10:04:09.181	0.47
64.05743	-21.41626	2.489	10:09:16.336	0.21

Latitude	Longitude	Depth (km)	Origin time	Magnitude
64.05804	-21.41531	2.240	10:10:43.386	0.95
64.05672	-21.41942	1.905	10:12:06.468	0.46
64.05743	-21.41546	2.145	10:14:26.104	0.78
64.15268	-21.35937	0	10:21:01.390	0.64
64.13087	-21.25178	0	10:23:37.597	1.14
64.12352	-21.22503	0.289	10:33:42.242	0.76
64.05975	-21.40598	4.716	10:52:37.177	1.3
64.04523	-21.41698	4.199	10:58:44.022	0.94
64.15182	-21.35936	0	11:02:41.077	0.5
64.14123	-21.29166	0	11:17:33.040	0.92
64.05537	-21.41743	4.054	11:29:39.168	1.66
64.12901	-21.24327	0	11:43:44.881	0.96
64.12663	-21.24445	0	11:54:20.371	1.01
64.05638	-21.41666	4.472	12:06:47.717	1.12
64.05680	-21.41915	4.216	12:32:55.137	1.23
64.05797	-21.41696	4.140	12:38:50.362	1.21
64.05927	-21.41502	2.429	12:40:22.783	1.55
64.05672	-21.41861	1.939	12:41:27.940	0.94
64.05883	-21.41397	2.420	12:48:30.971	0.98
64.05690	-21.41903	1.991	12:57:32.303	0.94
64.05857	-21.41656	2.274	13:14:23.458	1.57
64.04785	-21.41443	2.223	14:15:09.112	1.09
64.05901	-21.41761	2.059	14:19:11.410	1.62
64.05822	-21.41171	2.498	14:21:18.230	1.24
64.05672	-21.41379	1.802	14:24:44.079	0.78
64.05848	-21.41394	1.733	14:28:56.966	0.62
64.04864	-21.41550	2.455	14:31:08.509	0.68
64.05883	-21.41478	1.595	14:39:10.128	0.59
64.05646	-21.41477	2.016	14:44:02.796	1.52
64.05391	-21.42239	1.630	14:45:15.177	0.7
64.04829	-21.41949	2.145	15:03:53.408	0.71
64.05672	-21.41701	2.042	15:08:30.978	1.17
64.05602	-21.41695	1.733	15:15:13.394	1.26
64.05637	-21.41376	1.767	15:21:59.871	0.61
64.05496	-21.41525	1.973	15:24:22.139	1.03
64.05707	-21.41382	1.836	15:32:01.253	2.27